EBioMedicine 11 (2016) 138–150

Contents lists available at ScienceDirect

EBioMedicine

journal homepage: www.ebiomedicine.com

Research Paper

Dual Anti-Inflammatory and Anti-Angiogenic Action of miR-15a in Diabetic Retinopathy

Qi Wang [a], Svetlana Navitskaya [a], Harshini Chakravarthy [a], Chao Huang [a], Nermin Kady [a], Todd A. Lydic [a], Y. Eugene Chen [b], Ke-Jie Yin [c], Folami Lamoke Powell [d], Pamela M. Martin [d], Maria B. Grant [e], Julia V. Busik [a,*]

[a] Department of Physiology, Michigan State University, East Lansing, MI 48824, United States
[b] Department of Internal Medicine, University of Michigan, Ann Arbor, MI 48109, United States
[c] Department of Neurology, University of Pittsburgh School of Medicine, Pittsburgh, PA 15213, United States
[d] The Medical College of Georgia, at Augusta University, Augusta, GA 30912, United States
[e] Department of Ophthalmology, Indiana University School of Medicine, Indianapolis, IN 46202, United States

ARTICLE INFO

Article history:
Received 19 May 2016
Received in revised form 26 July 2016
Accepted 6 August 2016
Available online 8 August 2016

Keywords:
Diabetic retinopathy
microRNA
Sphingolipids
Dyslipidemias
Vascular system injuries

ABSTRACT

Activation of pro-inflammatory and pro-angiogenic pathways in the retina and the bone marrow contributes to pathogenesis of diabetic retinopathy. We identified miR-15a as key regulator of both pro-inflammatory and pro-angiogenic pathways through direct binding and inhibition of the central enzyme in the sphingolipid metabolism, ASM, and the pro-angiogenic growth factor, VEGF-A. miR-15a was downregulated in diabetic retina and bone marrow cells. Over-expression of miR-15a downregulated, and inhibition of miR-15a upregulated ASM and VEGF-A expression in retinal cells. In addition to retinal effects, migration and retinal vascular repair function was impaired in miR-15a inhibitor-treated circulating angiogenic cells (CAC). Diabetic mice overexpressing miR-15a under Tie-2 promoter had normalized retinal permeability compared to wild type littermates. Importantly, miR-15a overexpression led to modulation toward nondiabetic levels, rather than complete inhibition of ASM and VEGF-A providing therapeutic effect without detrimental consequences of ASM and VEGF-A deficiencies.

1. Introduction

Diabetic retinopathy (DR) is a leading cause of preventable blindness (Hammes, 2013; Prokofyeva and Zrenner, 2012). Recent progress in understanding of DR pathogenesis has led to significant advances in available pharmacotherapy; however a cure for DR has yet to be realized.

MicroRNAs (miRNAs) are small non-coding RNAs that non-perfectly anneal to target genes leading to gene silencing through cleavage, destabilization, or inhibition of mRNA translation. Each miRNA targets multiple genes, and, in turn, one gene may be regulated by multiple miRNAs. Hence, targeting one or a few miRNAs provides the unique opportunity to prevent expression of multiple genes and for development of RNA-based therapeutics. MiRNAs have been implicated in a variety of cellular processes, such as differentiation, proliferation, apoptosis, metabolism, and various signal transduction pathways (Chuang and Jones, 2007; He and Hannon, 2004). Expression of select miRNAs results in a post-transcriptional feedback control mechanism, which is believed to be involved in modulation of lipid and carbohydrate metabolism and inflammatory pathways (Feng et al., 2011; Poy et al., 2004), thereby potentially playing a key role in the pathogenesis of diabetes and its complications (Pandey et al., 2009). The role of miRNAs in DR pathogenesis is beginning to unfold. A recent study showed that 86 miRNAs were differentially expressed in the retina and 120 miRNAs differentially expressed in retinal endothelial cells isolated from diabetic rats when compared with control (Kovacs et al., 2011). Prominent among these were miRNAs controlled by the pathways playing an important role in the pathogenesis of diabetic retinopathy, namely NF-κB, VEGF, and p53-controlled miR-146, miR-31 and miR-34 (8). Consistent with this study, our previously published data demonstrated diabetes-induced dysregulation of daily rhythms of miR-146a and inflammatory pathways under miR-146a control in the retina (Wang et al., 2014). A growing body of literature identified miR-200b as miRNA contributing to VEGF upregulation and pathogenesis of diabetic retinopathy (McArthur et al., 2011; Suarez and Sessa, 2009; Chan et al., 2011). High glucose-induced downregulation of miR-152 led to increased expression levels of downstream VEGF, VRGFR-2, and TGFβ1 in HRECs through interaction with the (pro)renin receptor (Haque et al., 2015). Overexpression of miR-15b and miR-16 decreased TNFα and suppressor of cytokine signaling 3 (SOCS3)-mediated insulin resistance pathways while increasing insulin-like growth factor binding protein-3

* Corresponding author at: 3178 Biomedical Physical Science Building, East Lansing, MI-48824, United States.
E-mail address: busik@msu.edu (J.V. Busik).

http://dx.doi.org/10.1016/j.ebiom.2016.08.013

(IGFBP-3) levels in HRECs, and thus prevented hyperglycemia-induced apoptosis through activation of Akt phosphorylation and decreased cleavage of caspase 3 (Ye and Steinle, 2015).

Pro-inflammatory and pro-angiogenic factors are known to be activated in the diabetic retina. Prominent among these are the inflammatory cytokine, interleukin (IL)-1β, tumor necrosis factor α (TNFα) and IL-6; the adhesion molecules ICAM1 and VCAM1; and the growth factor, vascular endothelial growth factor A (VEGF-A). Elevated VEGF-A production results in increased retinal endothelial permeability and cell injury (Caldwell et al., 2005; Hu et al., 2013; Penn et al., 2008; Wang et al., 2015; Yang et al., 2013; Boyer et al., 2013; Harhaj et al., 2006; Simo et al., 2014). In addition to these key factors, we previously identified that acid sphingomyelinase (ASM), the enzyme converting sphingomyelin into pro-inflammatory and pro-apoptotic ceramide, is highly activated by diabetes in the retina (Opreanu et al., 2011). Endothelial cells, which represent a major source of ASM, had the highest level of activation of ASM in diabetic retina. The mechanism(s) of this activation remains largely unknown.

Retinal endothelial cell damage in diabetes (Joussen et al., 2001; Roy et al., 2015; Chronopoulos et al., 2011) is further confounded by inadequate vascular repair due, in part, to compromised function of the bone marrow (Busik et al., 2009; Caballero et al., 2007; Grant et al., 2002; Bhatwadekar et al., 2010; Chakravarthy et al., 2016). Bone marrow-derived circulating angiogenic cells (CACs) normally serve to mitigate endothelial injury, but are unable to participate in vascular repair in the retina of humans and rodents with chronic diabetes (Busik et al., 2009; Chakravarthy et al., 2016; Abu El-Asrar et al., 2011; Krady et al., 2005; Li Calzi et al., 2010; Tan et al., 2010; Liu et al., 2013; Sukmawati and Tanaka, 2015; Balaiya et al., 2014; Caballero et al., 2013). In human subjects we and others have used CD34 + cells as a marker of vascular reparative populations. We used the term CAC, however in the literature the term circulating progenitor cells (CPCs) is also used to define the same population of immature bone marrow (BM)–derived cells, mostly of hematopoietic origin, which have been associated with several aspects of CVDs, from diagnosis to therapy. In clinical studies, CACs/CPCs are generally defined by flow cytometry based on the surface expression of the hematopoietic stem cell markers CD34 and CD133 (Ingram et al., 2005). CPCs include phenotypes with vascular endothelial specification, usually called endothelial progenitor cells (EPCs). EPCs account for ≤15% of CPCs and are characterized by the co-expression of endothelial markers (mostly the type 2 vascular endothelial growth factor receptor KDR) (Fadini et al., 2008; Fadini et al., 2012). We have used a single marker, CD34, as Fadini et al. demonstrated that it was as predictive as using multiple markers (Rigato et al., 2016) and with isolation of human cells, in particular cells from diabetic patients, it is difficult to obtain sufficient numbers of cells and with the selection of each additional maker the number of cells isolated decreases, limiting what is available for study. In animal models, BM-derived progenitor cells contribute to vascular repair and include linage negative cells which are then positively selected for Sca-1.

In this study, we identified miR-15a as a miRNA that provides inhibition to both ASM and VEGF-A activation. MiR-15a was shown to be significantly downregulated in the blood of diabetic patients and T2D hyperglycemic Lep^{ob} mice (Zampetaki et al., 2010). Importantly, we provide an entirely new mechanism for the pathogenesis of diabetic retinopathy based on diabetes-induced downregulation of miR-15a expression leading to pro-inflammatory and pro-angiogenic changes in the diabetic retina due to unopposed activation of miR-15a target genes, ASM and VEGF-A.

2. Methods

2.1. Mouse Models and Rat Model

All procedures involving animal models were approved by Institutional Animal Care and Use Committee at MSU. The Tie-2 promoter driven miR-15a transgenic (Tie2-miR-15a TG) mice were from Dr. Y. Eugene Chen's group (Yin et al., 2012). C57BL/6J and C57BL/6-Tg(CAG-EGFP) mice were purchased from Jackson Laboratory. Eight week old male Tie2-miR-15a TG, C57BL/6J or C57BL/6-Tg(CAG-EGFP) mice were made diabetic by injections of 55 mg STZ (Sigma-Aldrich)/kg body weight for five consecutive days. Eight week old male Long Evans rats with body weights of 240 g were purchased from the Harlan laboratories (Haslett, MI, USA) and made diabetic by injections of 65 mg STZ (Sigma-Aldrich)/kg body weight for five consecutive days.

Control animals (mice and rats) received vehicle (100 mM citric acid buffer, pH = 4.5) injections. Body weight and blood glucose were monitored biweekly for these mice and rats during the induction of diabetes. Permeability was examined 4 weeks after the induction of diabetes to mimic early stage diabetic retinopathy for the control and STZ- induced Tie2-miR-15a TG mice. Sample and data were collected 8 weeks after the induction of diabetes for real-time PCR analysis and CACs isolation for the STZ- induced Tie2-miR-15a TG mice, C57BL/6J, C57BL/6-Tg(CAG-EGFP) mice and rats.

2.2. Cell Culture

Primary cultures of Human retinal endothelial cells (HRECs) were prepared from the retinas provided by National Disease Research Interchange (Philadelphia, PA) as previously described (Wang et al., 2014), or purchased from cell systems (Cell Systems, Kirkland, WA, USA). In brief, primary cultures of HRECs were obtained from at least three separate donors. Passages 3–6 were used in the experiments. Purity of the cells was determined using acetylated LDL uptake and Von Willebrand factor staining. Only 99% and higher purity HRECs preparations were used in the study. HRECs were grown in six-well plates coated with 0.1% gelatin in 2 ml growth medium/well consisting of Dulbecco's modified Eagle's medium/F12 (1:1 ratio, 5 mmol/l glucose) supplemented with 10% fetal bovine serum, 5% ECGS, 1% penicillin/streptomycin, and 1× ITS at 37 °C in humidified 95% air and 5% CO_2 until fully confluent. The cells were maintained at 37 °C in 5% CO_2 in a humidified cell culture incubator and passaged at a density of 40,000 to 100,000 cells/cm^2 in 75-cm^2 flasks. Passaged cells were plated to yield near-confluent cultures at the end of the experiments. Characteristics of the donors are summarized in Supplemental Table S1. Human retinal pigment epithelial cell line ARPE-19 cell culture (HRPE) cells were grown in 2 ml growth medium/well consisting of Dulbecco's modified Eagle's medium/F12 (1:1 ratio, 5 mmol/l glucose) supplemented with 10% fetal bovine serum, 1% penicillin/streptomycin, at 37 °C in humidified 95% air and 5% CO_2.

For tube formation assay, HRECs were seeded into tissue culture flasks coated with attachment factor (Cell Systems, Kirkland, WA, USA) and cultured in CSC Complete Medium (Cell Systems, Kirkland, WA, USA). When experimental conditions required serum-free medium, CSC Complete Serum-Free Medium was used. All cultures were incubated at 37 °C, 5% CO2, and 95% relative humidity (20.9% oxygen). Passages 6 to 8 were used for tube formation assay.

2.3. High Glucose Treatment and Transfection of HRPE Cells

HRPE cells were grown to 70% confluence in serum-free medium for 12 h and then treated with serum-free medium containing 5 mmol/l glucose (NG) or 25 mmol/l glucose (HG), respectively. After 24 h, NG or HG treated HRPE cells were transfected with 100 nM miRIDIAN miRNA mimic or antagomir for miR-15a and the negative controls (scrambled) (Dharmacon, Lafayette, CO). The transfected HRPE cells were maintained in serum-free medium with 5 mmol/l glucose or 25 mmol/l glucose respectively in 37 °C/5% CO_2 incubator. After 48 h, cells were harvested for total miRNA, RNA, lipid and proteins extraction. The results were confirmed by repeating experiment at least three times.

2.4. Real-Time PCR-Based miRNA Expression Profiling

HRECs isolated from retinas of diabetic (n = 6) and control donors (n = 6) were analyzed for the presence and differential expression of total 752 best characterized miRNAs in the human miRNA genome using human RT^2 miRNA PCR arrays (RT^2 Profiler; SABiosciences) according to the manufacturer's instructions. Data analysis was performed with the web-based software package for the miRNA PCR array system (http://www.sabiosciences.com/pcr/arrayanalysis.php) and TargetScan (http://www.targetscan.org/).

2.5. MiRNA and RNAi transfection

Cultured HRECs, CACs or HRECs were re-suspended in electroporation solution (Amaxa Biosystems, Gaithersburg, MD) to final concentration of 5×10^5 cells/100 μL. Then 100 μL cell suspension was mixed with 100 nM miRIDIAN miRNA mimic or antagomir for miR-15a and the negative controls (scrambled) (Dharmacon, Lafayette, CO) into the electroporation cuvette, and HRECs or CACs were electroporated (Nucleofactor program M-030; Amaxa Biosystems). The electroporated cells were maintained in supplemented medium in 37 °C/5% CO_2 incubator. After 48 h, cells were harvested for total miRNA, RNA and proteins extraction. The results were confirmed by repeating experiment at least three times.

2.6. Quantitative Real-Time PCR

Quantitative real-time PCR was performed to examine the expression levels of ASM and VEGF in rat retina (n = 6), HRECs (n = 6) and HRPE cells (n = 3). Specific primers used for each gene are listed in Supplemental Table S2. Expression levels of ASM and VEGF-A were normalized to cyclophilin A. TaqMan miRNA Assays were performed to examine the miRNA expression and the data were normalized to the expression of U87, U6 snRNA or RNU58B for rat, mice or human. Mouse expression levels of ASM, VEGF-A, ICAM-1, VCAM-1, IL-1β, IL-6 and TNF-α were examined using TaqMan gene expression assays and normalized to cyclophilin A.

2.7. Western Blotting

Samples were lysed using lysis buffer composed of 50 mM HEPES, 1 mM EGTA, 1.5 mM MgCl2, 150 mM NaCl, 10% glycerol and 1% Triton X-100, pH 7.5). Phosphatase inhibitor (1 mM Na4PPi, 10 mM NaF, 100 μM glycerophosphate, 1 mM Na3PO4) and protease inhibitor (Sigma-Aldrich, St. Louis, MO) were added fresh to the solution. A protein quantification assay (Bio-Rad Laboratories) was performed to determine the protein concentration for each sample. Proteins were loaded on NuPAGE gels containing 10% Bis-Tris (Life Technologies, Carlsbad, CA) and run for 1.5 h at 100 V. Resolved proteins were transferred to nitrocellulose membrane and stained with anti-ASM antibody at 1:1000 dilution (Cell Signaling), followed by Alexa-Fluor secondary antibody (Life Technologies, Carlsbad, CA). Immunoreactive bands were visualized using the Odyssey digital imaging program. ImageJ software was used for quantification of scanned blots.

2.8. Immunostaining and Quantitation of Ceramide Production

HRPE cells (3×10^4) were plated on cover-slips in 6-well plates 48 h prior to treatment. Rinse cells twice with PBS at room temperature before fixation. Cells were fixed in a solution of freshly prepared 4% paraformaldehyde for 10 min at room temperature and then permeabilized with ice cold acetone for 10 min. After pretreatments, cells were blocked with 5% normal goat sera (Jackson ImmunoResearch Laboratories Inc., West Grove, PA) for 2 h at room temperature and incubated with monoclonal mouse anti-ceramide antibody (Sigma-Aldrich, St. Louis, MO) at 1:50 in PBS with 1% BSA for 2 h at room temperature or overnight at 4 °C. After washing with PBS, the goat-mouse Texas Red conjugated secondary antibody (1:500) (Life Technologies, Carlsbad, CA) was incubated for 1 h at room temperature in the dark. Following washing with PBS three times, nuclei were stained for 10 min with DAPI (Sigma-Aldrich, St. Louis, MO). Slides were rinsed three times with distilled water and then postfixed with the Prolong Antifade Kit (Life Technologies, Carlsbad, CA), covered with glass coverslips, and subjected to fluorescent microscopy. The Texas Red fluorescence was visualized by excitation at 594 nm and collection of emissions at 618 nm, whereas the excitation and emission wavelengths for the DAPI detection were 350 and 460 nm, respectively. The images were viewed, and pictures were taken using a Nikon TE2000 fluorescence microscope equipped with Photometrics CoolSNAP HQ2 camera. All images were taken with matched exposure time for experimental and control sections and at least 5 different view areas were selected to collect images for each slide. The quantitation of ceramide was done using the MetaMorph imaging software (Molecular Devices, Downingtown, PA). The fluorescence intensity of ceramide signal in HRPE cells was normalized to the fluorescence intensity of DAPI in the nuclei. The autofluorescence was excluded from the analysis.

2.9. 3′UTR Luciferase Reporter Assay

Confirmation of miR-15a-binding to the putative 3′ untranslated region (UTR) binding-site of ASM utilized a dual luciferase reporter assay. HRPE cells at 80% confluency were transfected with 100 ng reporter vector pMir-SMPD1 3′UTR, a vector containing the 3′UTR clone of sphingomyelin phosphodiesterase 1 acid lysosomal (SMPD1), empty vector pMir empty-3′UTR or the mutant construct of pMir-SMPD1 3′ UTR, which was generated by replacing the seed regions of the miR-15a binding sites from 5′-TGCTGCT-3′ with 5′-TGTGACT-3′ mutation. All reporter vectors were purchased and constructed from OriGene Technologies (Rockville, MD, USA). Reporter vectors were co-transfected with mimic miR-15a (100 nM), or mimic scrambled negative control (Applied Biosystems), and a pGL4.74 (hRluc/TK) vector (Promega, Madison, WI) for normalization. DharmaFECT Duo (Dharmacon, Lafayette, CO) was used as the transfection reagent in serum free medium. Following 24 h incubation in transfection media, luciferase signal was measured using Dual-Luciferase Reporter Assay System according to manufacturer's instructions (Promega, Madison, WI).

2.10. Mass Spectrometry

1–5 million cells were subjected to monophasic lipid extraction. 10 μL of lipid sample was directly infused by nanoelectrospray ionization (nESI) into a high resolution/accurate mass Thermo Scientific model LTQ Orbitrap Velos mass spectrometer (San Jose, CA) using an Advion Triversa Nanomate nESI source (Advion, Ithaca, NY). High resolution mass spectra and Higher-Energy Collision Induced Dissociation (HCD-MS/MS) product ion spectra were acquired in positive ionization mode to confirm lipid headgroups and elucidate the sphingosyl backbone/acyl chain compositions of selected sphingolipid ions using the FT analyzer operating at 100,000 mass resolving power. Lipid identifications were achieved using the Lipid Mass Spectrum Analysis (LIMSA) v.1.0 software linear fit algorithm, in conjunction with a user-defined database of hypothetical lipid compounds for automated peak finding and correction of ^{13}C isotope effects. Relative quantification between samples was performed by normalization of target lipid ion peak areas to appropriate internal standards. Individual molecular species of ceramides are shown at magnification ranging from 20×–300×, and individual molecular species of sphingomyelin (SM) are shown under 10 × magnifications for clarity and to demonstrate the dynamic range of the Orbitrap mass spectrometer (Lydic et al., 2014).

2.11. In Situ Hybridizations (ISH) of miR15a

ISH was performed on frozen retinal section fixed in 4% PFA. MiRs were demasked by incubation with proteinase K for 30 min. Slides were incubated overnight at 58 °C using double (5′and 3′) DIG-labeled locked nucleic acid miRNA detection probes specific for mouse miR-15a (Exiqon; Woburn, MA) coupled with DyLight 594 anti-DIG fluorescent antibody (Vector Laboratories; Burlingame, CA). Slides were then washed in 2×, 1× and .1× concentrations of sodium citrate (SSC) buffers at 58 °C, 53 °C, and 37 °C, respectively, followed by a one hour incubation with anti-DIG (Roche Diagnostics, Indianapolis, IN) and mounting with Fluoromount. Images were captured by light microscopy using Zeiss Axioplan2.

2.12. Retinal Vascular Permeability

Two months after induction of diabetes in the littermate wild-type control and Tie2-miR-15a TG mice, *in vivo* vascular permeability in the retina was measured. Briefly, mice were injected with FITC- albumin (0.5 mg in 100 μL PBS) (Sigma-Aldrich, St. Louis, MO). After two hours, blood was collected from each mouse and centrifuged to obtain plasma; the animal was perfused with 1% formaldehyde and enucleated. Retinas were removed, flat-mounted with four slits and kept on glass slides with Fluoromount mounting medium (Sigma-Aldrich, St. Louis, MO). Images were acquired using an Olympus FluoView 1000 scanning laser confocal microscope and at least 5 different view areas were selected to collect images for each sample. Retinas were disrupted mechanically and cleared by centrifugation. FITC-albumin in supernatant was quantified using spectrofluorometer and normalized to plasma fluorescence (Kielczewski et al., 2011).

2.13. Retinal Ischemia-Reperfusion (I/R)

All procedures involving the animal models adhered to the ARVO statement for the Use of Animals in Ophthalmic and Vision Research. I/R were created by temporal increase in intraocular pressure to 90 mm Hg as described previously (Zheng et al., 2007). The intravitreal injection procedure was performed 7 days after retinal I/R.

2.14. CAC Isolation and Migration

Age matched male control (n = 10) or diabetic gfp^+ mice (n = 10) were euthanized and tibias and femurs were collected. Ice-cold PBS was used to flush bones, and single cell suspension was made. Ammonium chloride (STEMCELL technologies) was used to eliminate erythrocytes contaminating the bone marrow cells. Next, negative selection using magnetic beads (STEMCELL Technologies) was used to isolate hematopoietic stem/progenitor cells from mouse bone marrow, and positive selection for Sca-1 (STEMCELL Technologies) was used to obtain Lin-Sca + progenitor cells. Enriched progenitor cells were kept in a cell culture incubator with 5% CO_2 at 37 °C overnight, in EGM-2 media with SingleQuot supplements and growth factors added (Lonza) to enable recovery from the enrichment process. The wells below were loaded with 100 nM SDF-1, 10% FBS as positive control or PBS as negative control. The migration set-up was incubated with 5% CO_2 at 37 °C for 4 h. To determine the number of migrated cells, fluorescence emitted at 550 nm was measured using a microplate reader. Samples were analyzed in triplicate and data expressed as percentage relative to positive control ± SEM (Tikhonenko et al., 2013). The cells isolated by this protocol were formerly called EPCs (endothelial progenitor cells).The terminology has now been updated to CACs (circulating angiogenic cells), which is more reflective of the function of these cells.

2.15. Reendothelialization of Retinal Vasculature

10,000 $Lin^- Sca^+ gfp^+$ CACs isolated from control or diabetic gfp^+ mice were treated with miR-15a mimics or inhibitors, or corresponding controls for 48 h and then were injected intravitreously using 33-gauge Hamilton syringe into eyes isolated from control or I/R injured mice (7 days after I/R). After seven days to allow progenitor cells homing to retinal vessels, mice were sacrificed, eyes removed, pierced with a 30-gauge needle, fixed in 4% paraformaldehyde for 1 h, and washed in PBS. Retinas were isolated and flat-mounted with four slits and kept on glass slides with fluoromount mounting medium (Sigma-Aldrich, St. Louis, MO). Retinas in the glass slides were then permeabilized overnight at 4 °C in HEPES-buffered saline containing 0.1% Tween 20 and 1% BSA. Vasculature was stained with rabbit anti-collagen IV (abcam) diluted 1:400, followed by PBS wash. Secondary antibody chicken anti-rabbit (Alexa Fluor 594, Invitrogen) (red), diluted 1:1000 was used to detect collagen IV. Coverslips were mounted on slides using ProLong® Gold Antifade Mountan (Life Technologies, CARLSBAD, CA). Single XY confocal fluorescence images were acquired using the Olympus FluoView FV1000 Confocal Laser Scanning Microscope (Olympus America, Inc., Center Valley, PA) configured on a fully automated IX81 inverted microscope using a 20× UPlanSApo (NA 0.75) objective. The confocal fluorescence images were sequentially scanned to prevent fluorescence emission crossover. The GFP (displayed in green) was excited using the 488 nm Argon gas laser line and the fluorescence emission was collected using a 522.5/45 nm band pass filter. Collagen IV labeled with Alexa Fluor 594 (displayed in red) was excited using the 559 nm solid state laser and the fluorescence emission was collected using a 620/100 nm band pass filter. All images were taken with matched exposure times for experimental and control sections and at least 5 different view areas were selected to collect images for each retina. The co-localization of gfp^+ cells (green) and collagen IV (red) associated with retinal vasculature (yellow) was used to evaluate the incorporation ability of CACs. The quantitation of co-localization was done using the MetaMorph imaging software (Molecular Devices, Downingtown, PA). The fluorescence intensity of retinal vasculature (yellow) in the mouse retina was measured. The autofluorescence of the section was excluded from the analysis.

2.16. Matrigel In Vitro HRECs Tube Formation Assay

Tube formation assay was performed using the BD BioCoat Angiogenesis System-Endothelial Cells Tube Formation Matrigel Matrix 96-well plate Matrigel (BD Biosciences Discovery Labware, Bedford, MA) as manual provided by manufacture. Briefly, a 96-well culture plate was coated with 100 μL of matrigel per well and allowed to polymerise for 30 min at 37 °C. HRECs treated with miRNA mimic or antagomir for miR-15a and the negative controls (scrambled) at a density of 2×10^4 cells $well^{-1}$ were plated in 0.3 ml of CSC Complete Serum-Free Medium for 18 h at 37 °C. The images of tubes were taken in ×10 magnifications using a Nikon TE2000 fluorescence microscope equipped with Photometrics CoolSNAP HQ2 camera. All images were taken with matched exposure time for experimental and control sections and at least 5 different view areas were selected to collect images for each well. The quantitation of tube formation was done using the MetaMorph imaging software (Molecular Devices, Downingtown, PA). Samples were analyzed in triplicate and data expressed the number of tubes as percentage relative to control ± SEM.

2.17. Statistical Analysis

All of results were confirmed by repeating experiment at least three times. Data are expressed as the mean ± SE for gene expression. Two-way ANOVA with post hoc Tukey test (GraphPad Prism5, GraphPad Software, San Diego, CA) was used to compare the data obtained from independent samples. Significance was established at $P < 0.05$.

3. Results

3.1. Decreased miR-15a Leads to Increased ASM Expression in Retinal Cells in Diabetes

We have previously demonstrated that ASM expression is highly upregulated in diabetic retinas and this is associated with activation of inflammatory cytokines (Opreanu et al., 2011). To determine if altered miRNA control could contribute to ASM upregulation in diabetes, we used Target Scan (http://www.targetscan.org/) to identify miRNAs that have target sequence for the 3′UTR of ASM mRNA. We found six predicted miRNAs: miR-497, miR-15a, miR-15b, miR-424, miR-16 and miR-195.

We next performed the miRNA array to determine differentially expressed miRNAs in the HRECs isolated from control and diabetic donors. We used RT^2 miRNA PCR arrays followed by individual qPCR validations for selected miRNAs and found 60 miRNAs that were >2.5 fold upregulated and 16 miRNAs downregulated in HRECs isolated from diabetic *vs.* control eyes (Fig. 1A). Notably, the miRNA PCR array data showed that miR-15a was down-regulated in HRECs isolated from the diabetic donors relative to the control donors, but there was no effect of diabetes on the other five miRNAs targeting ASM (Fig. 1A, B). Furthermore, qRT-PCR verification of selected miRNAs demonstrated that miR-133b was increased while miR-15a, miR-10a and miR-10b were decreased in HRECs from retina of diabetic donors (n = 6) compared with control donors (n = 6), confirming the array data (Fig. 1B). Notably, miR-15a was the only miRNA differentially expressed between control and diabetic HRECs among six miRNAs predicted to control ASM (miR-497, miR-15a, miR-15b, miR-424, miR-16 and miR-195).

In agreement with our previous studies (Opreanu et al., 2011), HRECs had the highest ASM expression level among retinal cells (Opreanu et al., 2011). Interestingly, higher basal ASM mRNA level corresponded to lower miR-15a levels in HRECs compared to HRPE cells (Fig. 2A). In support of Target Scan and miRNA array data, analysis of HRECs isolated from diabetic donors (n = 6) demonstrated reduction of miR-15a (Fig. 1B) with concomitant increase of ASM compared to control (Fig. 2B). Importantly, in agreement with our previous data (Busik et al., 2008), high glucose did not affect miR-15a and ASM expression in endothelial cells (data not shown), thus control and diabetic cells were used to determine the role of diabetic environment in HREC.

Critical to diabetic retinopathy is the function of the retinal pigment epithelium (RPE), the cell type responsible for the generation of the outer blood retinal barrier. As RPE cells are highly sensitive to glucose concentration, high glucose treatment was used to mimic diabetic condition in HRPE cells. We examined the effect of high glucose on expression of miR-15a and ASM in HRPE. HRPE cells treated with 25 mmol/l glucose had decreased miR-15a expression and increased ASM expression compared with 5 mmol/l glucose treated HRPE cells (Fig. 2C).

3.2. miR-15a Directly Inhibits the Expression of ASM by Binding 3′UTR of ASM mRNA

To determine whether miR-15a directly recognizes the 3′UTR of ASM mRNA, we cloned the predicted target site of miR-15a or a mutant

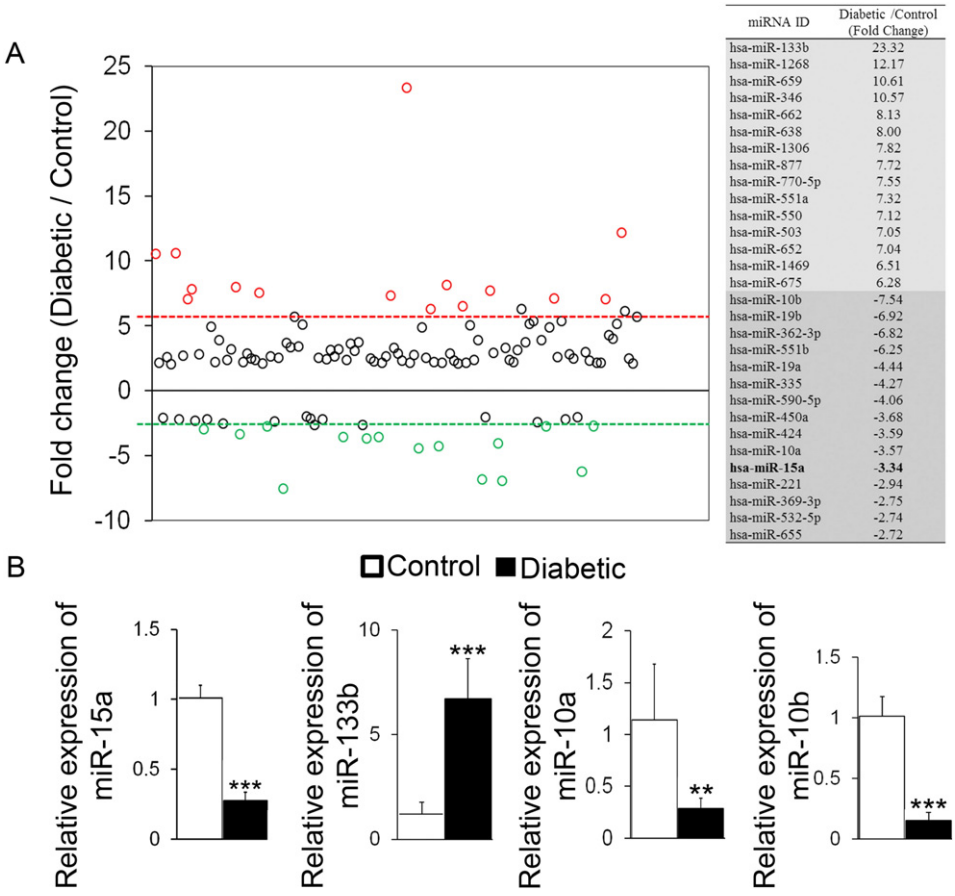

miRNA ID	Diabetic /Control (Fold Change)
hsa-miR-133b	23.32
hsa-miR-1268	12.17
hsa-miR-659	10.61
hsa-miR-346	10.57
hsa-miR-662	8.13
hsa-miR-638	8.00
hsa-miR-1306	7.82
hsa-miR-877	7.72
hsa-miR-770-5p	7.55
hsa-miR-551a	7.32
hsa-miR-550	7.12
hsa-miR-503	7.05
hsa-miR-652	7.04
hsa-miR-1469	6.51
hsa-miR-675	6.28
hsa-miR-10b	-7.54
hsa-miR-19b	-6.92
hsa-miR-362-3p	-6.82
hsa-miR-551b	-6.25
hsa-miR-19a	-4.44
hsa-miR-335	-4.27
hsa-miR-590-5p	-4.06
hsa-miR-450a	-3.68
hsa-miR-424	-3.59
hsa-miR-10a	-3.57
hsa-miR-15a	**-3.34**
hsa-miR-221	-2.94
hsa-miR-369-3p	-2.75
hsa-miR-532-5p	-2.74
hsa-miR-655	-2.72

Fig. 1. Identification and verification of miRNAs differentially expressed in the HRECs isolated from control and diabetic donors (A) Human RT^2 miRNA PCR arrays were used to profile the differential expression of total miRNAs in HRECs isolated from control (n = 6) and diabetic donors (n = 6). MiRNAs upregulated or downregulated by >2.5-fold relative to control are shown. MiRNAs marked with red or green were top 15 miRNAs upregulated or downregulated by diabetes, respectively. (B) Relative expressions of miR-15a and selected miRNAs were determined by qPCR to validate the array result. Data are mean ± SEM (n = 6). *** $P < 0.001$; ** $P < 0.01$; * $P < 0.05$; not significant at $P > 0.05$.

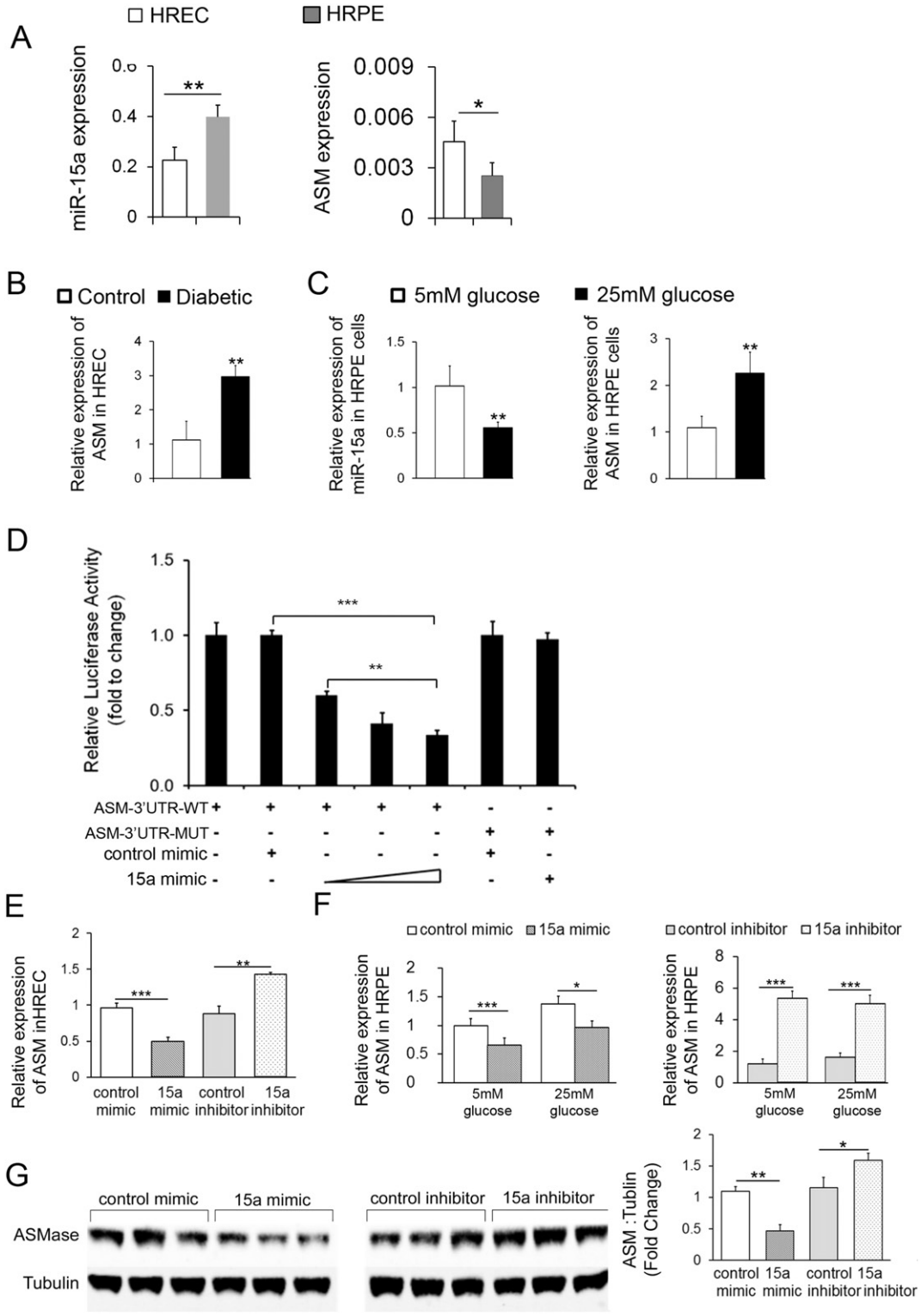

Fig. 2. MiR-15a negatively regulates the expression of ASM by direct targeting 3′UTR of ASM mRNA (A) Expression profiles of miR-15a and ASM were determined by real-time PCR in HRECs from control donors (n = 6) and HRPE cells (n = 3). (B) ASM expression was examined in HRECs from diabetic donors (n = 6) compared with control donors (n = 6). (C) Expression profiles of miR-15a and ASM were detected by real-time PCR in HRPE treated with 25 mmol/l glucose for 24 h compared with 5 mmol/l glucose (n = 3). (D) HRPE cells were co-transfected with wild type human ASM 3′UTR or mutant ASM 3′UTR (200 ng) luciferase reporters and miR-15a mimic in increasing concentrations (30, 50 and 100 nM). Mutant human ASM 3′UTR and control mimic served as negative controls. Luciferase activity was measured 48 h post-transfection. (E) Real-time PCR analysis of ASM mRNA level after miR-15a mimic or inhibitor delivery in HRECs. (F) Real-time PCR analysis of ASM mRNA level after miR-15a mimic or inhibitor delivery in HRPE cells under normal and high glucose conditions for 24 h (n = 3). (G) Western blot analysis of ASM protein expression after miR-15a mimic or inhibitor delivery in HRPE cells under normal and high glucose conditions for 48 h (n = 3). α-tubulin serves as a loading control. Representative blots are from three independent experiments. Quantification of band intensity is relative to control. Data are mean ± SEM (n = 3). *** $P < 0.001$; ** $P < 0.01$; * $P < 0.05$; not significant at $P > 0.05$.

target site sequence downstream of the pMir-Target luciferase reporter gene vector. When the ASM 3′UTR wild-type or mutant luciferase reporter gene vector was co-transfected with miR-15a, the luciferase activity of the ASM 3′UTR wild-type vector resulted in dose-dependent decrease compared with the mutant vector (Fig. 2D). Next, miR-15a mimics or inhibitors were used to test the effect of diabetes and/or high glucose regulation of ASM in HRECs and HRPE. The validated individual negative miRIDIAN mimic or inhibitor controls were used to assure specificity of miRNA modulation experiment. As expected, the over-expression of miR-15a was able to markedly downregulate the expression of ASM mRNA in HRECs and HRPE under normal and elevated glucose conditions. Furthermore, the miR-15a inhibitor was able to upregulate the expression of ASM mRNA in HRECs and HRPE under both normal and elevated glucose conditions (Fig. 2E and F). Importantly, ASM protein expression in HRPE cells was decreased compared to control mimic-transfected cells; however, miR-15a inhibitor increased ASM protein expression by in HRPE cells (Fig. 2G).

3.3. MiR-15a Controls Retinal Ceramide Production

To further confirm the effect of miR-15a on sphingolipid metabolism, immunoreactivity of ceramide using anti-ceramide antibody was examined in HRPE cells after either the overexpression or inhibition of miR-15a using miRNA mimics and inhibitors, respectively. As shown in Fig. 3, delivery of miR-15a mimics in HRPE cells suppressed the increase in ceramide observed following the high glucose (Fig. 3A). In contrast, miR-15a inhibitors further increased ceramide levels (Fig. 3B).

Since endothelial cells represent a major source of ASM and a primary cell type affected by DR, we next used 10–12 weeks old male Tie2-miR-15a TG mice to evaluate the effect of endothelial miR-15a on retinal ceramide production. The sphingolipid profile of Tie2-miR-15a TG mouse retina was compared to wild type (top) and complete ASM knockout (middle) mouse retina (Fig. 3C) (n = 5 per group). As expected, $ASM^{-/-}$ retina demonstrated dramatic increase in sphingomyelin species and concomitant decrease in ceramide species (blue bold labels) (Fig. 3C). Tie2-miR-15a TG mouse retina demonstrated intermediate sphingolipid phenotype with decreased ceramide levels, but not as pronounced changes in SM profiles. The ratio of total retina ceramide to total SM content was significantly decreased in $ASM^{-/-}$, as well as Tie2-miR-15a TG mice retinas (Fig. 3C).

3.4. MiR-15a Negatively Regulates the Expression Level of VEGF-A

Recently, miR-15a has been identified as a key regulator of pro-angiogenic pathway through direct binding to VEGF-A (but not VEGF-B, C and D) 3′UTR (Yin et al., 2012). Therefore, we next examined the effect of miR-15a on VEGF-A in human retinal cells. VEGF-A mRNA levels were upregulated in HRECs isolated from diabetic donors (n = 6) and in high glucose-treated HRPE. These changes were associated with concomitant downregulation of miR-15a (Figs. 2A, 4A and B). Over-expression of miR-15a by miR-15a mimic markedly downregulated while miR-15a inhibitor upregulated VEGF-A expression in HRECs compared to mimic and inhibitor controls (Fig. 4C). When HRPE cells were treated with high glucose and miR-15a mimics or inhibitors for 48 h, over-expression of miR-15a markedly downregulated the expression of VEGF-A mRNA in HRPE under normal and high glucose conditions (Fig. 4D). The miR-15a inhibitor induced upregulation of the VEGF-A mRNA expression in HRPE under normal and high glucose conditions (Fig. 4D). Importantly, VEGF-A protein expression in HRPE was decreased compared to control mimic-transfected cells; miR-15a inhibitor increased VEGF-A protein expression (Fig. 4E). Taken together, these results suggest that miR-15a controls basal VEGF-A expression in HRECs and basal and high glucose-induced VEGF-A expression in HRPE (Fig. 4A–E, Supplemental Fig. S1A–B).

3.5. Overexpression of miR-15a in Bone Marrow Improves CAC Release, Migration and Homing to Retinal Vasculature

Accumulating evidence suggests that bone marrow-derived CACs in diabetes lose their ability to home to areas of injury and mediate vascular repair, resulting in retinal vascular pathology (Busik et al., 2009; Caballero et al., 2007). CACs isolated from the blood of diabetic patients with DR ($CD34^{+}$) (Supplemental Table S3), and diabetic mouse models showed decreased miR-15a expression levels (Fig. 5A). To assess the effect of changes in miR-15a on the repair capacity of CACs, we assessed their ability to home to injured retinal vessels in the mouse ischemia-reperfusion (I/R) model. When control and miR-15a mimic-treated-healthy CACs were injected into the vitreous of diabetic mice, we observed their participation in vessel repair as demonstrated by colocalization of green (gfp^{+} CACs) and red (retinal vasculature staining). As shown in Fig. 5B, control and miR-15a mimic-treated healthy CACs demonstrated robust vascular repair function, whereas the repair function was impaired in miR-15a inhibitor-treated CACs. Diabetic CACs lose this repair ability and fail to home to areas of retinal injury; however, miR-15a mimic-treated diabetic CACs recovered their repair ability (Fig. 5B and Table 1). Next, the effect of miR-15a on migration of CACs was examined. In agreement with the *in vivo* retinal vascular repair studies, healthy control and miR-15a mimic-treated CACs demonstrated robust migration capacity, but migration was impaired in diabetic and in miR-15a inhibitor treated CACs. The migration was normalized in miR-15a mimic-treated diabetic CACs (Fig. 5C). As expected, there was no effect miR-15a mimics on migration and repair in healthy CAC controls, and, conversely, there was no effect miR-15a inhibitors in diabetic CACs (Fig. 5C).

To evaluate the role of miR-15a in HRECs tube formation, we performed *in vitro* matrigel tube formation assay. There was no effect of either 15a mimics (p-value = 0.098) or 15a inhibitors (p-value = 0.152) on HRECs tube formation as compared to scrambled control (Fig. 5D and E).

3.6. miR-15a Expression Profile in Control and Diabetic Retina

Next, we determined the miR-15a expression in control and STZ-induced diabetic rat retinas. As shown in Figs. 5 and 6A, decreased miR-15a expression in retinas of diabetic rat (n = 6) was followed by increased expression levels of ASM and VEGF-A. Importantly, *in situ* hybridization of mouse retina demonstrated that miR-15a level was markedly reduced in diabetic retina as compared to control (n = 4) (Fig. 6B).

3.6.1. Overexpression of miR-15a Prevented Retinal Inflammation and Vascular Damage In Vivo

Male Tie2-miR-15a TG mice (8–10 weeks old, n = 8) were used to test the effect of overexpressed miR-15a on retinal inflammation and vascular damage. The retinal expression profile of miR-15a, ASM, VEGF, IL6, IL1β and TNFα in Tie2-miR-15a TG mice and littermate controls are shown in Fig. 6C. Overexpression of miR-15a as observed in retinas of the Tie2-miR-15a TG mice (n = 8) resulted in decreased expression levels of ASM and VEGF-A (Fig. 6C). The expression levels

Fig. 3. MiR-15a regulates ceramide production in retina and retinal cells The immunoreactivity of ceramide was examined in HRPE cells under normal and high glucose conditions for 24 h (n = 3) after overexpression or inhibition of miR-15a by (A) miR mimics and (B) inhibitors respectively. Representative images show the immunoreactivity of ceramide. Signal detection and image acquisition were performed by fluorescence microscopy using Photometrics CoolSNAP HQ2 camera. The fluorescence intensity (red) of ceramide in the HRPE cells was normalized to DAPI (blue) nuclei staining and quantified in triplicates using the MetaMorph imaging software. (C) Orbitrap high resolution/accurate mass spectra were collected in positive ionization mode from monophasic lipid extracts of WT, ASM −/−, and Tie2-miR-15a TG mouse retina (n = 5 per group). Data are mean ± SEM. *** $P < 0.001$; ** $P < 0.01$; * $P < 0.05$; not significant at $P > 0.05$.

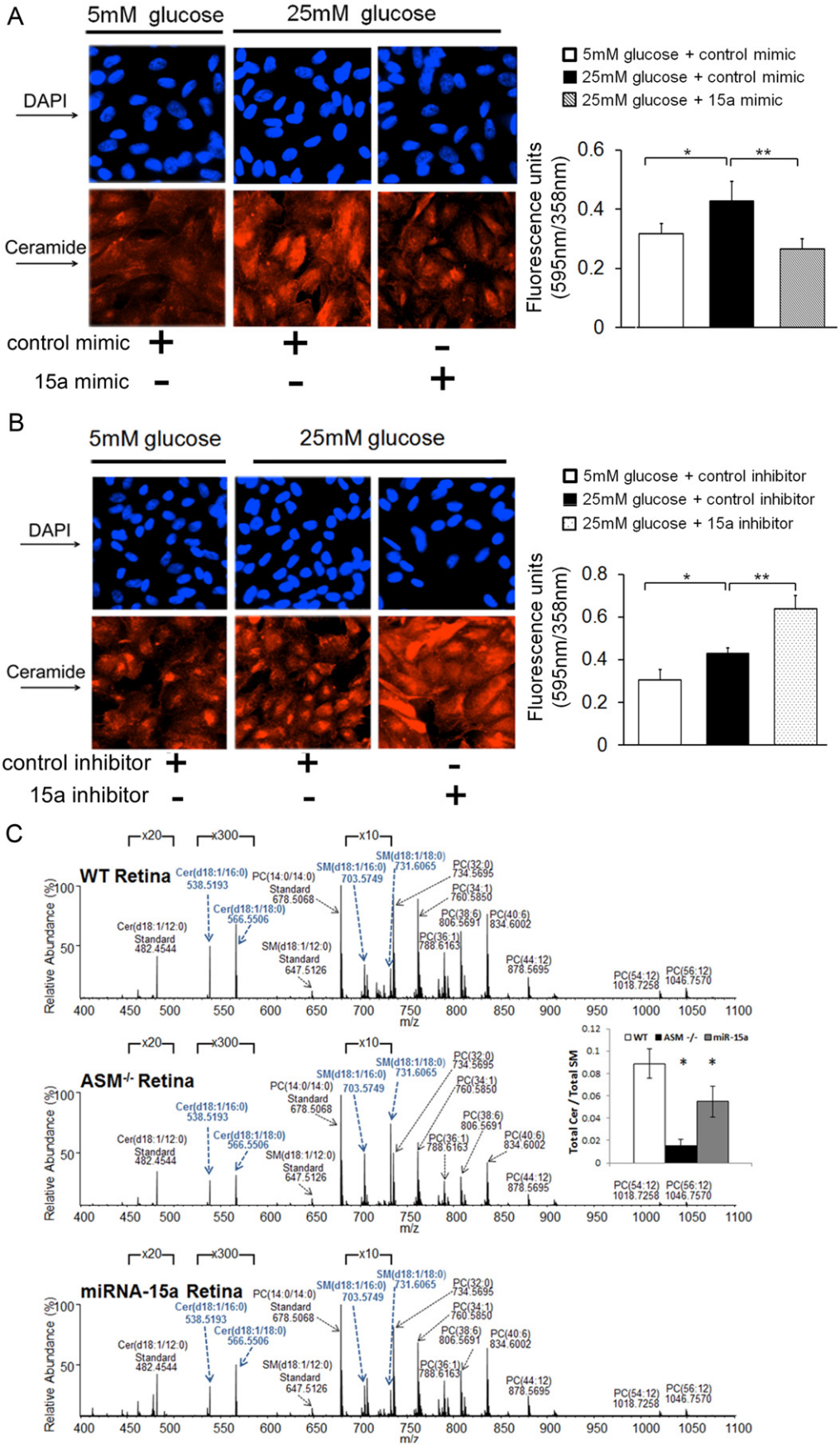
A
5mM glucose
25mM glucose
DAPI
Ceramide
control mimic + + -
15a mimic - - +
5mM glucose + control mimic
25mM glucose + control mimic
25mM glucose + 15a mimic
Fluorescence units (595nm/358nm)
B
5mM glucose
25mM glucose
DAPI
Ceramide
control inhibitor + + -
15a inhibitor - - +
5mM glucose + control inhibitor
25mM glucose + control inhibitor
25mM glucose + 15a inhibitor
Fluorescence units (595nm/358nm)
C
WT Retina
ASM-/- Retina
miRNA-15a Retina
Relative Abundance (%)
m/z
Total Cer / Total SM
WT
ASM -/-
miR-15a

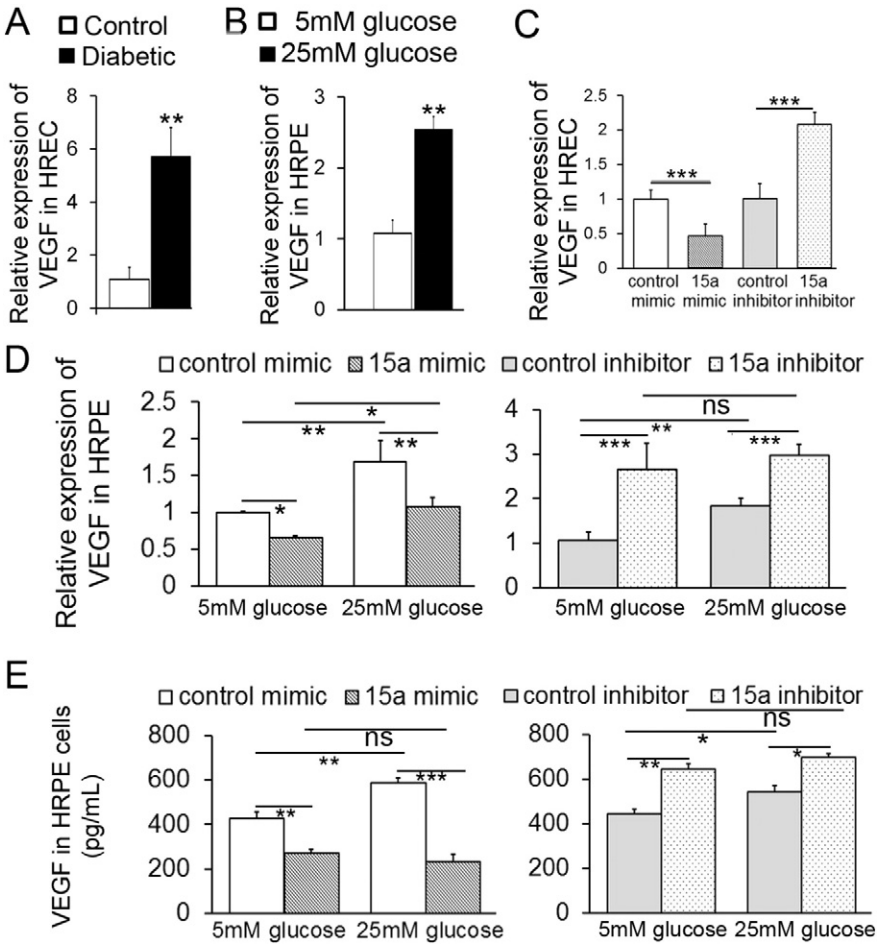

Fig. 4. MiR-15a negatively regulates the expression of VEGF-A in HRPE and HRECs Expression levels of VEGF-A were determined by real-time PCR in (A)HRECs from diabetic donors (n = 6) compared with control donors (n = 6) and (B) HRPE cells treated with 25 mmol/l glucose for 24 h compared with 5 mmol/l glucose (n = 3). RT-PCR analysis of VEGF-A mRNA levels after miR-15a mimic or inhibitor delivery in (C) HRECs and (D) HRPE cells under normal and high glucose conditions for 24 h (n = 3). (E) ELISA analysis of VEGF-A protein expression after miR-15a mimic or inhibitor delivery in HRPE cells under normal and high glucose conditions for 48 h (n = 3). Data are mean ± SEM (n = 3). *** $P < 0.001$; ** $P < 0.01$; * $P < 0.05$; not significant at $P > 0.05$.

of IL6, IL1β and TNFα were trending lower, however there were no statistically significant differences in these transcripts. To further illustrate the beneficial effect of overexpression of miR-15a on retinal vascular damage, vascular permeability was measured in the retinas of these different cohorts. Vascular permeability as assessed by leakage of FITC-albumin was increased in diabetic retinas compared to control (n = 6) and this increase was prevented in Tie2-miR-15a TG mice (Fig. 6D).

4. Discussion

Diabetic retinopathy is a complex disorder that involves both systemic and retinal tissue-specific initiating factors and cell types. A number of hyperglycemia- and dyslipidemia-activated pathways leading to retinal endothelial cell and CAC dysfunction have been identified (Busik et al., 2009; Grant et al., 2002; Bhatwadekar et al., 2010; Chakravarthy et al., 2016; Abu El-Asrar et al., 2011; Li Calzi et al., 2010; Tan et al., 2010; Liu et al., 2013; Caballero et al., 2013). Prominent among these are pathways promoting the increase of pro-inflammatory cytokines, pro-inflammatory lipids and pro-angiogenic factors. Dysregulation of these pathways is hypothesized to involve miRNAs. These small non-coding RNAs anneal imperfectly to target genes and simultaneously control translation and transcription. Single species of miRNA can interact with a wide range of target transcripts. Several miRNA classes have been shown to contribute to diabetes and diabetic complications (Pandey et al., 2009; Zampetaki et al., 2010), including diabetic retinopathy (Suarez and Sessa, 2009).

Our previous studies identified dysfunctional sphingolipid metabolism, due to pathological activation of ASM in diabetic retina and bone marrow, as an important metabolic insult contributing to pro-inflammatory changes in the retina and development of diabetic retinopathy (Opreanu et al., 2011; Tikhonenko et al., 2013; Busik et al., 2012; Chakravarthy et al., 2015; Opreanu et al., 2010). Endothelial cells are the major source of ASM and we observed the highest activation of ASM in retinal endothelial cells in diabetes compared to other retinal cells (Opreanu et al., 2011; Tikhonenko et al., 2013; Opreanu et al., 2010). VEGF is another well-known factor that is increased in the diabetic retina leading to increased retinal vascular permeability and ultimately neovascularization in some species. Intravitreal anti-VEGF treatments provide the most successful diabetic retinopathy therapy to date. Both ASM and VEGF-A are, however, essential for normal retinal function and their inhibition may lead to serious consequences, such as lysosomal storage disease (Opreanu et al., 2011; Chen et al., 2014; Kaarniranta et al., 2013) for ASM and damage to cone photoreceptors and choroidal vasculature for VEGF. Indeed, complete ASM deficiency leads to neurodegeneration, activation of microglia and loss of retinal function in ASM −/− mice (Dannhausen et al., 2015; Horinouchi et al., 1995). Based on the ability of miRNAs to function more like a rheostat than an on/off switch as they work by "dimming", rather than complete silencing of gene expression, we reasoned that miRNAs would provide a feasible therapeutic approach, particularly for targets such as ASM and

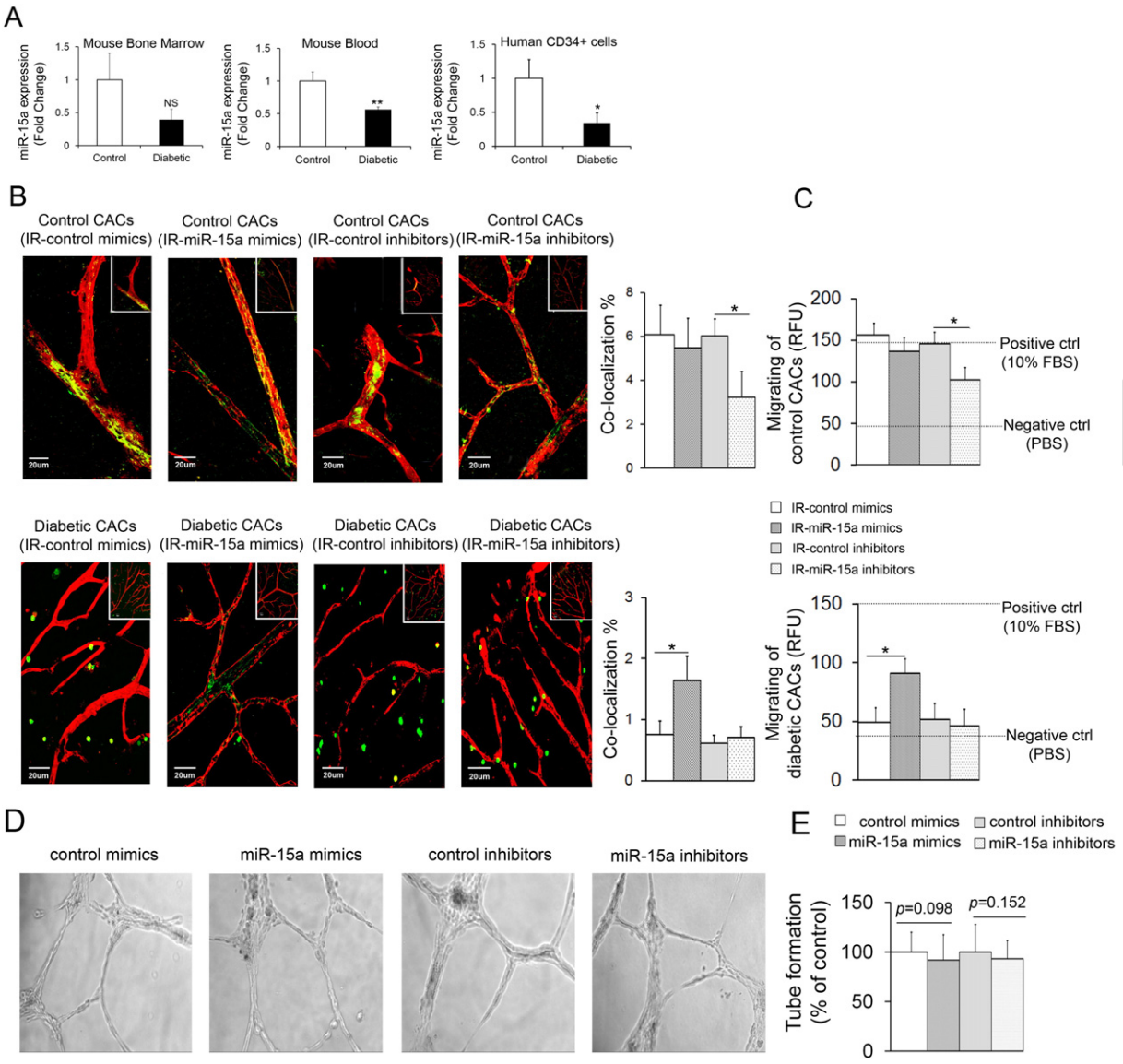

Fig. 5. Upregulation of miR-15a in bone marrow improves CAC release, migration and homing to retinal vasculature (A) The expression levels of miR-15a were determined in mouse bone marrow (n = 6 per group), blood (n = 6 per group) and in human $CD34^+$ cells isolated from diabetic patients (n = 8 per group) with DR. (B, C) CACs (green) isolated from control or STZ-induced diabetic gfp^+ mice (duration of diabetes 8 weeks, n = 10 per group) were treated with control mimic, miR-15a mimic, control inhibitor or miR-15a inhibitor. Wild-type mice undergoing I/R model received intravitreal injections of CACs treated with mimic or inhibitor for miR-15a and the negative controls (scrambled) (n = 6 for each treatment). The retinal vasculature was stained with anti-collagen IV antibody (red). Confocal images of retina isolated from I/R injured mice treated with control mimic, miR-15a mimic, control inhibitor or miR-15a inhibitor and the quantification of co-localization of gfp^+ cells associated with retinal vasculature (yellow) were shown in B. CACs migration towards either 100 nM SDF-1, PBS (negative control), or 10% FBS (positive control) were shown in C. RFU, relative fluorescence units. Data are mean ± SEM (n = 6). *** $P < 0.001$; ** $P < 0.01$; * $P < 0.05$; not significant at $P > 0.05$. (D, E) The *in vitro* tube formation assay was performed in HRECs after overexpression or inhibition of miR-15a by miR mimics and inhibitors respectively using Matrigel Matrix 96-well plate. (D) Photomicrographs of representative assays for control mimics, 15a mimics, control inhibitor and 15a inhibitor. The images of tubes were taken in ×10 magnifications and at least 5 different fields were randomly selected to collect images from each well. (E) Quantitative data for tube formation expressed as number of closed network of vessel-like tubes as percentage relative to control. Data is mean ± SEM (n = 3).

VEGF-A where partial reductions rather than complete inhibition, is desirable.

In search of miRNAs that have combined anti-inflammatory and anti-angiogenic potential, we first performed the miRNA array to determine differentially expressed miRNAs in the HRECs isolated from control and diabetic donors. Among all the miRNAs downregulated in diabetic donors, miR-15a was the only one that had the predicted anti-inflammatory and anti-angiogenic targets, ASM and VEGF-A. Moreover, miR-15a was the most significantly downregulated miRNA in the blood of diabetic patients and T2D hyperglycemic Lep^{ob} mice (Zampetaki et al., 2010). Importantly, miR-15a was reported to directly target 3′UTR and inhibit VEGF-A and FGF2 (Yin et al., 2012) providing an important novel mechanism for control of angiogenesis. ASM regulation by miR-15a had not been previously confirmed, thus we performed 3′ UTR of ASM mutation studies. These studies demonstrated that miR-15a negatively regulates ASM expression through direct targeting the 3′UTR of ASM mRNA.

Table 1
The effect of miR-15a on migration and repair capacity of CACs.

	miR-15a Mimic	miR-15a Inhibitor
Control CACs	No effect	Impaired migration and repair function
Diabetic CACs	Improved migration and repair function	No effect

Angiogenesis is strictly controlled by a balance between pro-angiogenic and anti-angiogenic factors. Regulation of key angiogenic factors, VEGF-A and FGF2, by miR-15a is important in maintaining this delicate balance. Disruption of this balance could favor pathological angiogenesis, such as seen in diabetic retinopathy. Indeed, miR-15a was shown to be reduced in pathological angiogenesis in hindlimb ischemia

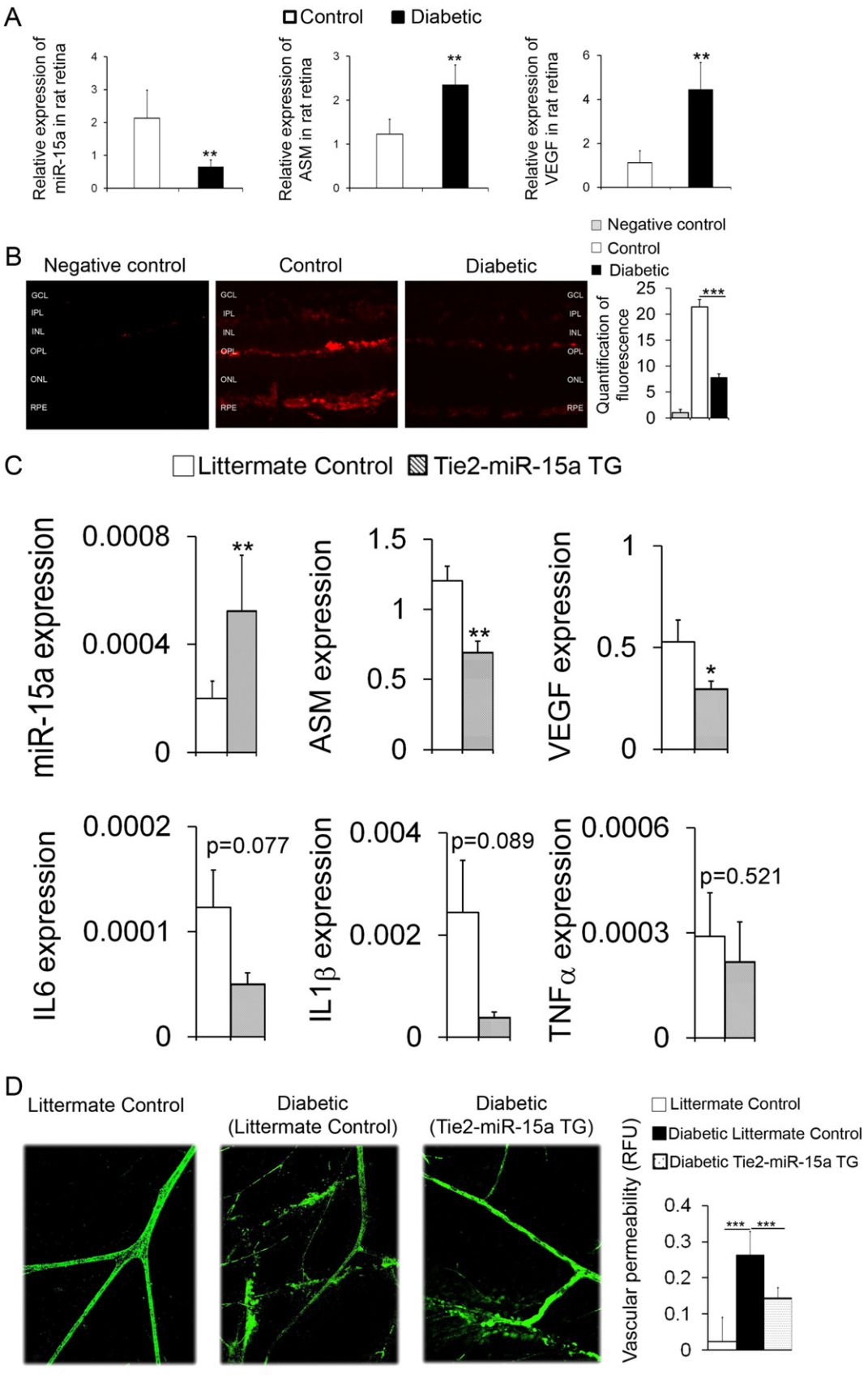

model (Yin et al., 2012). Our data confirm this finding and demonstrate that miR-15a could thus be used to simultaneously control both sphingolipid metabolism and VEGF-A production.

Reduction in miR-15a expression can affect retinal vascular pathology at two different levels. First, decrease in miR-15a has a direct effect on the retina leading to ASM activation, low-grade chronic inflammation and VEGF-A production, resulting in increased retinal endothelial permeability and cell injury. In addition, low miR-15a leads to high ASM expression and ceramide production in bone marrow-derived CACs in diabetes. Previously, we demonstrated that CACs with high ASM and ceramide levels have diminished migration, homing to the injured tissue and repair function (Opreanu et al., 2011; Tikhonenko et al., 2013; Busik et al., 2012; Chakravarthy et al., 2015; Opreanu et al., 2010). Furthermore, the combination of retinal endothelial cell injury and failed attempts by CACs to repair injured retinal capillaries, eventually results in progression to the vaso-degenerative stage of diabetic (Bhatwadekar et al., 2010; Chakravarthy et al., 2016; Abu El-Asrar et al., 2011; Li Calzi et al., 2010; Tan et al., 2010; Sukmawati and Tanaka, 2015; Caballero et al., 2013; Chakravarthy et al., 2015).

In this study, we used Tie-2 miR-15a transgenic mice that have increased miR-15a expression in the endothelial cells and bone marrow progenitor cells. To further distinguish retinal and bone marrow specific effects of miR-15a, we used CACs isolated from control and diabetic animals treated with miR-15a mimics and inhibitors. As expected, CACs isolated from diabetic animals had low miR-15a expression, leading to decreased migration and repair function compared to control. Treating diabetic CACs with miR-15a mimics improved their migration and repair function. Control CACs treated with miR-15a inhibitors lost their migration and repair capacity similar to diabetic CACs.

5. Conclusion

This study identified novel mechanism of DR pathogenesis through downregulation of miR-15a in the retina and bone marrow cells. Manipulation of miR-15a to simultaneously control sphingolipid metabolism and pro-angiogenic pathways through direct regulation of ASM and VEGF-A production in the diabetic retina and bone marrow provides a unique and effective “combination therapy” approach that will add to the pharmacological armamentarium of drug therapies for diabetic retinopathy. Our studies support the use of this novel approach for treatment of diabetic retinopathy and other disabling conditions associated with activation of multiple deleterious signaling pathways.

Author Contributions

Q.W. designed the experiment, performed the study and wrote the manuscript. S.N.N., H.C., C.H., N.K., T.A.L., Y.E.C., K.J.Y., P.M.M., and F.L. performed animal model experiments. M.B.G. contributed to development of the study designs and experimental concepts proposed in the study, the discussion and reviewed and edited the manuscript. J.V.B. designed the experiment, performed the study and reviewed and edited the manuscript.

Acknowledgments

We thank Juvenile Diabetes Research Foundation (JDRF) Fellowship JDRF 3-PDF-2014-108-A-N to Q.W, National Institutes of Health (NIH) grant EY-01-6077, Michigan AgBioResearch grant MICL02163 to JVB, NIH grants EY-07739 and EY-12601 to MBG, Jean P Schultz Research Award to JVB, and NIH grant DK-09-0730 to MBG and JVB. Mass spectrometry analysis was provided by the Molecular Metabolism and Disease Collaborative Mass Spectrometry Core at Michigan State University. JVB is the guarantor of this work and, as such, had full access to all the data in the study and takes responsibility for the integrity of the data and the accuracy of the data analysis. All of funding sources had no role in study design, data collection, data analysis, interpretation, writing of the manuscript or the decision to submit it for publication. I have not been paid to write this article by a pharmaceutical company or other agency.

Appendix A. Supplementary Data

Supplementary data to this article can be found online at http://dx.doi.org/10.1016/j.ebiom.2016.08.013.

References

Abu El-Asrar, A.M., Struyf, S., Verbeke, H., Van Damme, J., Geboes, K., 2011. Circulating bone-marrow-derived endothelial precursor cells contribute to neovascularization in diabetic epiretinal membranes. Acta Ophthalmol. 89, 222–228.

Balaiya, S., Grant, M.B., Priluck, J., Chalam, K.V., 2014. Growth factors/chemokines in diabetic vitreous and aqueous alter the function of bone marrow-derived progenitor (CD34(+)) cells in humans. Am. J. Physiol. Endocrinol. Metab. 307, E695–E702.

Bhatwadekar, A.D., Shaw, L.C., Grant, M.B., 2010. Promise of endothelial progenitor cell for treatment of diabetic retinopathy. Expert. Rev. Endocrinol. Metab. 5, 29–37.

Boyer, D.S., Hopkins, J.J., Sorof, J., Ehrlich, J.S., 2013. Anti-vascular endothelial growth factor therapy for diabetic macular edema. Ther. Adv. Endocrinol. Metab. 4, 151–169.

Busik, J.V., Mohr, S., Grant, M.B., 2008. Hyperglycemia-induced reactive oxygen species toxicity to endothelial cells is dependent on paracrine mediators. Diabetes 57, 1952–1965.

Busik, J.V., Tikhonenko, M., Bhatwadekar, A., Opreanu, M., Yakubova, N., Caballero, S., Player, D., Nakagawa, T., Afzal, A., Kielczewski, J., et al., 2009. Diabetic retinopathy is associated with bone marrow neuropathy and a depressed peripheral clock. J. Exp. Med. 206, 2897–2906.

Busik, J.V., Esselman, W.J., Reid, G.E., 2012. Examining the role of lipid mediators in diabetic retinopathy. Clin. Lipidol. 7, 661–675.

Caballero, S., Sengupta, N., Afzal, A., Chang, K.H., Calzi, S.L., Guberski, D.L., Kern, T.S., Grant, M.B., 2007. Ischemic vascular damage can be repaired by healthy, but not diabetic, endothelial progenitor cells. Diabetes 56, 960–967.

Caballero, S., Hazra, S., Bhatwadekar, A., Li Calzi, S., Paradiso, L.J., Miller, L.P., Chang, L.J., Kern, T.S., Grant, M.B., 2013. Circulating mononuclear progenitor cells: differential roles for subpopulations in repair of retinal vascular injury. Invest. Ophthalmol. Vis. Sci. 54, 3000–3009.

Caldwell, R.B., Bartoli, M., Behzadian, M.A., El-Remessy, A.E., Al-Shabrawey, M., Platt, D.H., Liou, G.I., Caldwell, R.W., 2005. Vascular endothelial growth factor and diabetic retinopathy: role of oxidative stress. Curr. Drug Targets 6, 511–524.

Chakravarthy, H., Navitskaya, S., O'Reilly, S., Gallimore, J., Mize, H., Beli, E., Wang, Q., Kady, N., Huang, C., Blanchard, G.J., et al., 2015. Role of acid sphingomyelinase in shifting the balance between pro-inflammatory and reparative bone marrow cells in diabetic retinopathy. Stem Cells.

Chakravarthy, H., Beli, E., Navitskaya, S., O'Reilly, S., Wang, Q., Kady, N., Huang, C., Grant, M.B., Busik, J.V., 2016. Imbalances in mobilization and activation of pro-inflammatory and vascular reparative bone marrow-derived cells in diabetic retinopathy. PLoS One 11, e0146829.

Chan, Y.C., Khanna, S., Roy, S., Sen, C.K., 2011. miR-200b targets Ets-1 and is down-regulated by hypoxia to induce angiogenic response of endothelial cells. J. Biol. Chem. 286, 2047–2056.

Chen, H., Chan, A.Y., Stone, D.U., Mandal, N.A., 2014. Beyond the cherry-red spot: Ocular manifestations of sphingolipid-mediated neurodegenerative and inflammatory disorders. Surv. Ophthalmol. 59, 64–76.

Chronopoulos, A., Trudeau, K., Roy, S., Huang, H., Vinores, S.A., 2011. High glucose-induced altered basement membrane composition and structure increases trans-endothelial permeability: implications for diabetic retinopathy. Curr. Eye Res. 36, 747–753.

Chuang, J.C., Jones, P.A., 2007. Epigenetics and microRNAs. Pediatr. Res. 61, 24R–29R.

Dannhausen, K., Karlstetter, M., Caramoy, A., Volz, C., Jagle, H., Liebisch, G., Utermohlen, O., Langmann, T., 2015. Acid sphingomyelinase (aSMase) deficiency leads to abnormal microglia behavior and disturbed retinal function. Biochem. Biophys. Res. Commun. 464, 434–440.

Fig. 6. MiR-15a overexpression in Tie-2 miR-15a TG mice prevents diabetes-induced increase in retinal vascular permeability. (A) Expression profiling of miR-15a, ASM and VEGF-A in retinas from control and STZ-induced diabetic rats (duration of diabetes for 8 weeks, n = 10 per group). (B) In situ hybridization was used to determine the location of miR-15a in the retinas of control and STZ-induced diabetic mice. n = 4 per group. (C) Expression profiling of miR-15a, ASM, VEGF, IL6, IL1β and TNFα in retinas isolated from littermate control and Tie2-miR-15a TG mice. n = 8 per group. (D) Permeability of retinas isolated from littermate control, STZ-induced diabetic littermate control and Tie2-miR-15a TG mice (duration of diabetes H 4 weeks, n = 6 per group) was examined. Leakage of FITC-albumin from blood vessels was measured. Data are mean ± SEM. *** $P < 0.001$; ** $P < 0.01$; * $P < 0.05$; not significant at $P > 0.05$.

Fadini, G.P., Baesso, I., Albiero, M., Sartore, S., Agostini, C., Avogaro, A., 2008. Technical notes on endothelial progenitor cells: ways to escape from the knowledge plateau. Atherosclerosis 197, 496–503.
Fadini, G.P., Losordo, D., Dimmeler, S., 2012. Critical reevaluation of endothelial progenitor cell phenotypes for therapeutic and diagnostic use. Circ. Res. 110, 624–637.
Feng, B.A., Chen, S.L., McArthur, K., Wu, Y.X., Sen, S., Ding, Q.M., Feldman, R.D., Chakrabarti, S., 2011. miR-146a-mediated extracellular matrix protein production in chronic diabetes complications. Diabetes 60, 2975–2984.
Grant, M.B., May, W.S., Caballero, S., Brown, G.A.J., Guthrie, S.M., Mames, R.N., Byrne, B.J., Vaught, T., Spoerri, P.E., Peck, A.B., et al., 2002. Adult hematopoietic stem cells provide functional hemangioblast activity during retinal neovascularization. Nat. Med. 8, 607–612.
Hammes, H.P., 2013. Optimal treatment of diabetic retinopathy. Ther. Adv. Endocrinol. Metab. 4, 61–71.
Haque, R., Hur, E.H., Farrell, A.N., Iuvone, P.M., Howell, J.C., 2015. MicroRNA-152 represses VEGF and TGFbeta1 expressions through post-transcriptional inhibition of (Pro)renin receptor in human retinal endothelial cells. Mol. Vis. 21, 224–235.
Harhaj, N.S., Felinski, E.A., Wolpert, E.B., Sundstrom, J.M., Gardner, T.W., Antonetti, D.A., 2006. VEGF activation of protein kinase C stimulates occludin phosphorylation and contributes to endothelial permeability. Invest. Ophthalmol. Vis. Sci. 47, 5106–5115.
He, L., Hannon, G.J., 2004. Micrornas: small RNAs with a big role in gene regulation. Nat. Rev. Genet. 5, 522–531.
Horinouchi, K., Erlich, S., Perl, D.P., Ferlinz, K., Bisgaier, C.L., Sandhoff, K., Desnick, R.J., Stewart, C.L., Schuchman, E.H., 1995. Acid sphingomyelinase deficient mice: a model of types A and B Niemann-Pick disease. Nat. Genet. 10, 288–293.
Hu, Y., Chen, Y., Ding, L., He, X., Takahashi, Y., Gao, Y., Shen, W., Cheng, R., Chen, Q., Qi, X., et al., 2013. Pathogenic role of diabetes-induced PPAR-alpha down-regulation in microvascular dysfunction. Proc. Natl. Acad. Sci. U. S. A. 110, 15401–15406.
Ingram, D.A., Caplice, N.M., Yoder, M.C., 2005. Unresolved questions, changing definitions, and novel paradigms for defining endothelial progenitor cells. Blood 106, 1525–1531.
Joussen, A.M., Murata, T., Tsujikawa, A., Kirchhof, B., Bursell, S.E., Adamis, A.P., 2001. Leukocyte-mediated endothelial cell injury and death in the diabetic retina. Am. J. Pathol. 158, 147–152.
Kaarniranta, K., Sinha, D., Blasiak, J., Kauppinen, A., Vereb, Z., Salminen, A., Boulton, M.E., Petrovski, G., 2013. Autophagy and heterophagy dysregulation leads to retinal pigment epithelium dysfunction and development of age-related macular degeneration. Autophagy 9, 973–984.
Kielczewski, J.L., Calzi, S.L., Shaw, L.C., Cai, J., Qi, X.P., Ruan, Q., Wu, L., Liu, L., Hu, P., Chan-Ling, T., et al., 2011. Free insulin-like growth factor binding protein-3 (IGFBP-3) reduces retinal vascular permeability in association with a reduction of acid sphingomyelinase (ASMase). Invest. Ophthalmol. Vis. Sci. 52, 8278–8286.
Kovacs, B., Lumayag, S., Cowan, C., Xu, S., 2011. MicroRNAs in early diabetic retinopathy in streptozotocin-induced diabetic rats. Invest. Ophthalmol. Vis. Sci. 52, 4402–4409.
Krady, J.K., Basu, A., Allen, C.M., Xu, Y., LaNoue, K.F., Gardner, T.W., Levison, S.W., 2005. Minocycline reduces proinflammatory cytokine expression, microglial activation, and caspase-3 activation in a rodent model of diabetic retinopathy. Diabetes 54, 1559–1565.
Li Calzi, S., Neu, M.B., Shaw, L.C., Grant, M.B., 2010. Endothelial progenitor dysfunction in the pathogenesis of diabetic retinopathy: treatment concept to correct diabetes-associated deficits. EPMA J. 1, 88–100.
Liu, X., McBride, J., Zhou, Y., Liu, Z., Ma, J.X., 2013. Regulation of endothelial progenitor cell release by Wnt signaling in bone marrow. Invest. Ophthalmol. Vis. Sci. 54, 7386–7394.
Lydic, T.A., Busik, J.V., Reid, G.E., 2014. A monophasic extraction strategy for the simultaneous lipidome analysis of polar and nonpolar retina lipids. J. Lipid Res. 55, 1797–1809.
McArthur, K., Feng, B., Wu, Y., Chen, S., Chakrabarti, S., 2011. MicroRNA-200b regulates vascular endothelial growth factor-mediated alterations in diabetic retinopathy. Diabetes 60, 1314–1323.
Opreanu, M., Lydic, T.A., Reid, G.E., McSorley, K.M., Esselman, W.J., Busik, J.V., 2010. Inhibition of cytokine signaling in human retinal endothelial cells through downregulation of sphingomyelinases by docosahexaenoic acid. Invest. Ophthalmol. Vis. Sci. 51, 3253–3263.
Opreanu, M., Tikhonenko, M., Bozack, S., Lydic, T.A., Reid, G.E., McSorley, K.M., Sochacki, A., Perez, G.I., Esselman, W.J., Kern, T., et al., 2011. The unconventional role of acid sphingomyelinase in regulation of retinal microangiopathy in diabetic human and animal models. Diabetes 60, 2370–2378.
Pandey, A.K., Agarwal, P., Kaur, K., Datta, M., 2009. MicroRNAs in diabetes: tiny players in big disease. Cell. Physiol. Biochem. 23, 221–232.
Penn, J.S., Madan, A., Caldwell, R.B., Bartoli, M., Caldwell, R.W., Hartnett, M.E., 2008. Vascular endothelial growth factor in eye disease. Prog. Retin. Eye Res. 27, 331–371.
Poy, M.N., Eliasson, L., Krutzfeldt, J., Kuwajima, S., Ma, X.S., MacDonald, P.E., Pfeffer, S., Tuschl, T., Rajewsky, N., Rorsman, P., et al., 2004. A pancreatic islet-specific microRNA regulates insulin secretion. Nature 432, 226–230.
Prokofyeva, E., Zrenner, E., 2012. Epidemiology of major eye diseases leading to blindness in Europe: a literature review. Ophthalmic Res. 47, 171–188.
Rigato, M., Avogaro, A., Fadini, G.P., 2016. Levels of circulating progenitor cells, cardiovascular outcomes and death: a meta-analysis of prospective observational studies. Circ. Res. 118, 1930–1939.
Roy, S., Kim, D., Hernandez, C., Simo, R., 2015. Beneficial effects of fenofibric acid on overexpression of extracellular matrix components, COX-2, and impairment of endothelial permeability associated with diabetic retinopathy. Exp. Eye Res. 140, 124–129.
Simo, R., Sundstrom, J.M., Antonetti, D.A., 2014. Ocular anti-VEGF therapy for diabetic retinopathy: the role of VEGF in the pathogenesis of diabetic retinopathy. Diabetes Care 37, 893–899.
Suarez, Y., Sessa, W.C., 2009. MicroRNAs as novel regulators of angiogenesis. Circ. Res. 104, 442–454.
Sukmawati, D., Tanaka, R., 2015. Introduction to next generation of endothelial progenitor cell therapy: a promise in vascular medicine. Am. J. Transl. Res. 7, 411–421.
Tan, K., Lessieur, E., Cutler, A., Nerone, P., Vasanji, A., Asosingh, K., Erzurum, S., Anand-Apte, B., 2010. Impaired function of circulating CD34(+) CD45(−) cells in patients with proliferative diabetic retinopathy. Exp. Eye Res. 91, 229–237.
Tikhonenko, M., Lydic, T.A., Opreanu, M., Calzi, S.L., Bozack, S., McSorley, K.M., Sochacki, A.L., Faber, M.S., Hazra, S., Duclos, S., et al., 2013. N-3 polyunsaturated fatty acids prevent diabetic retinopathy by inhibition of retinal vascular damage and enhanced endothelial progenitor cell reparative function. PLoS One 8.
Wang, Q., Bozack, S.N., Yan, Y., Boulton, M.E., Grant, M.B., Busik, J.V., 2014. Regulation of retinal inflammation by rhythmic expression of MiR-146a in diabetic retina. Invest. Ophthalmol. Vis. Sci. 55, 3986–3994.
Wang, Y., Yang, C., Gu, Q., Sims, M., Gu, W., Pfeffer, L.M., Yue, J., 2015. KLF4 promotes angiogenesis by activating VEGF signaling in human retinal microvascular endothelial cells. PLoS One 10, e0130341.
Yang, W., Yu, X., Zhang, Q., Lu, Q., Wang, J., Cui, W., Zheng, Y., Wang, X., Luo, D., 2013. Attenuation of streptozotocin-induced diabetic retinopathy with low molecular weight fucoidan via inhibition of vascular endothelial growth factor. Exp. Eye Res. 115, 96–105.
Ye, E.A., Steinle, J.J., 2015. miR-15b/16 protects primary human retinal microvascular endothelial cells against hyperglycemia-induced increases in tumor necrosis factor alpha and suppressor of cytokine signaling 3. J. Neuroinflammation 12, 44.
Yin, K.J., Olsen, K., Hamblin, M., Zhang, J.F., Schwendeman, S.P., Chen, Y.E., 2012. Vascular endothelial cell-specific microRNA-15a inhibits angiogenesis in hindlimb ischemia. J. Biol. Chem. 287, 27055–27064.
Zampetaki, A., Kiechl, S., Drozdov, I., Willeit, P., Mayr, U., Prokopi, M., Mayr, A., Weger, S., Oberhollenzer, F., Bonora, E., et al., 2010. Plasma microRNA profiling reveals loss of endothelial MiR-126 and other microRNAs in type 2 diabetes. Circ. Res. 107 (810-U359).
Zheng, L., Gong, B., Hatala, D.A., Kern, T.S., 2007. Retinal ischemia and reperfusion causes capillary degeneration: similarities to diabetes. Invest. Ophthalmol. Vis. Sci. 48, 361–367.